Effect of Rolling Bearing on Dynamic Characteristics of Seal-Rotor System

Yuegang Luo
College of Mechanical and Electronic Engineering, Dalian Minzu University
Key Laboratory of Intelligent Perception and Advanced Control of State Ethnic Affairs Commission, Dalian Minzu University
Dalian China
luoyg@dlnu.edu.cn

Pengfei Wang
College of Mechanical and Electronic Engineering, Dalian Minzu University
Key Laboratory of Intelligent Perception and Advanced Control of State Ethnic Affairs Commission, Dalian Minzu University
Dalian China
2861014893@qq.com

Haifeng Jia
College of Mechanical and Electronic Engineering, Dalian Minzu University
Key Laboratory of Intelligent Perception and Advanced Control of State Ethnic Affairs Commission, Dalian Minzu University
Dalian China
1742971914@qq.com

Hao Xu
College of Mechanical and Electronic Engineering, Dalian Minzu University
Key Laboratory of Intelligent Perception and Advanced Control of State Ethnic Affairs Commission, Dalian Minzu University
Dalian China
528235288@qq.com

Chenyong Wang
College of Mechanical and Electronic Engineering, Dalian Minzu University
Key Laboratory of Intelligent Perception and Advanced Control of State Ethnic Affairs Commission, Dalian Minzu University
Dalian China
932332150@qq.com

***Abstract*—For problem which the vibration of rolling bearing-rotor system in the aero-engine with sealing device, the dynamic model of sealing-rotor system supported by angular contact ball bearings was established based on the finite element theory, Muzynska seal force model and rolling bearing force model. Vibration response characteristics of the system were obtained by the method of Newmark-β numerical integration. The results show that the phenomenon of frequency locking occurs in the rotor system after airflow excitation, accompanied by the characteristics of combination frequencies; when the bearing clearance is larger, the unstable vibration caused by the larger bearing clearance can be restrained to some extent by the airflow excitation force at lower rotating speed. The chaotic characteristics of the bearing end are gradually strengthened by the influence of the airflow excitation. In the absence of airflow force, the amplitude of rotor is increased by enhancing the bearing clearance and contact angle, and the amplitude is reduced by raising balls number properly. In the presence of airflow force, the number of balls, bearing clearance and contact angle have a little effect on the amplitude due to the influence of airflow excitation. Therefore, the factors such as bearing skidding and axial load are considered, in order to reduce vibration, it is necessary to properly improve the processing accuracy of the rotating shaft in the bearing installation and select the bearing type with smaller contact angle. The results provide a theoretical basis for fault diagnosis with airflow excited vibration and rolling bearings selection of this kind of rotating machinery.**

Keywords- labyrinth seal; rolling bearing; rotor system; airflow excited vibration; combination frequency; finite element

I. INTRODUCTION

The labyrinth sealing device is an effective sealing structure widely installed in modern aero-engine, steam turbine and other power rotating machinery structures. As a non-contact seal, it has the characteristics of simple structure, low energy consumption, long service life and no lubrication. Its function is to reduce the fluid leakage loss [1]. For the rotor system with

National Natural Science Foundation of China (No.51875085)

978-1-7281-0860-5/19/$31.00 ©2019 IEEE

labyrinth seals, the gas flow excitation is occurred easily and lead to the rotor instability made by enhancing the working speed, increasing rotor flexibility and higher parameter seals. Therefore, in order to enhance the stability and safety of this kind of system, studying the dynamic characteristics of the rotor system under the action of airflow excitation force and analyzing the influence rules of some typical parameters are significant.

In the field of rotor dynamics with seal, a great number of researchers have studied it. It can be summarized as two main aspects, one is the model establishment of sealing force and the other is the study of dynamic characteristics. In terms of the model, it can be divided into two parts: the parametric analytical model and the numerical calculation model. The Thomas-Alford model and Muzynska seal force model are included by the parametric analytical model, the numerical calculation model is dominated by the control volume model. In addition, in recent years, Computational Fluid Dynamics (CFD) method has been used by more and more scholars to calculate and analyze the flow field in seals [1], such as Xin Y et al.[2]; A new thermoelastic flow model for labyrinth seals was proposed by Cangioli F et al.[3]. In the research of dynamic characteristics, firstly, the stability of sealing system was studied by solving the dynamic characteristic coefficient. For example, when the pressure ratio is relatively low and the rotational speed is relatively high, the phenomenon that increasing centrifugation is not conducive to system stability was found by Subramanian S et al.[4]. The second is to study the influence factors of seal leakage in order to reduce leakage, such as literatures [5-7]. The third is to study the non-linear vibration problems including airflow excited vibration, sliding bearings, rubbing, cracks and other coupling faults, which can be seen in references [8-11].

In the current literatures, the steam turbine rotor is mostly taken as the research object, the model is simplified to Jeffcott rotor, and the sliding bearing is used as the support. However, there are few studies on the dynamic characteristics of the rotor seal structure with rolling bearings as the representative of the aero-engine rotor, and the effect of the seal structure parameters about the airflow excitation are mostly analyzed. There are few reports on the effects of the parameters with the rolling bearings on the dynamic characteristics about the rotor with the seal structure. In this paper, the front-end intake fan rotor of a turbofan aero-engine is taken as the research object. In order to highlight the main contradiction, the blade is simplified to a disk. Considering the influence of gyroscopic effect, the finite element model of the seal-rolling bearing-cantilever rotor system is established by Muszynska seal force model and the support force model of rolling bearing. The system is simulated and analyzed by the Newmark-β numerical algorithm. The vibration characteristics of airflow excited vibration and the influence of different rolling bearing parameters such as bearing clearance, number of balls and contact angle on the vibration characteristics of the system are analyzed, which provide a theoretical basis for the design and selection of rolling bearings for this type of rotary machinery.

II. MODEL OF SEAL-ROLLING BEARING-ROTOR SYSTEM

A. Dynamic Model of Rotor System

As shown in Fig.1, the total length of the labyrinth seal-rotor system is 845 mm, of which the extended end is 286 mm. The rotating shaft is a stepped shaft, the left side is a sealed disc with a diameter of 200 mm and a length of 100 mm. The outer part of the sealed disc is a sealed stator with the same length as it. There are two staggered labyrinth seals on the disc, the length of both two seals are 15 mm, and the air intake hole is located in sealed stator. At the center, the right end of the rotor is an elastic diaphragm coupling with an intermediate shaft, which conveys the torque from the motor output shaft to the rotor to drive its rotation. The system is divided into 27 axle segments by finite element method. The small points in the diagram represent nodes, and the number of nodes is numerically represented. There are 28 nodes in the system. The disk mass is concentrated on the nodes 6-9. The left and right bearing nodes are 13 and 17 respectively. Two groups of 7013C/DB angular contact ball bearings are installed in pairs. Timoshenko beam element is used to simulate the axle segment. There are two section nodes A and B in it. Each node has six degrees of freedom, translating and rotating along the x, y and z directions. The corresponding translational displacements and rotating angles are expressed as $x_A(x_B)$, $y_A(y_B)$, $z_A(z_B)$ and $\theta_{xA}(\theta_{xB})$, $\theta_{yA}(\theta_{yB})$, $\theta_{zA}(\theta_{zB})$, respectively. Radial vibration is studied only, and axial vibration is not considered, so the displacement and rotation angle of z axis are neglected. The displacement vector of the axis element is:

$$\boldsymbol{u_i} = [x_A, y_A, \theta_{xA}, \theta_{yA}, x_B, y_B, \theta_{xB}, \theta_{yB}]^{\mathrm{T}} \tag{1}$$

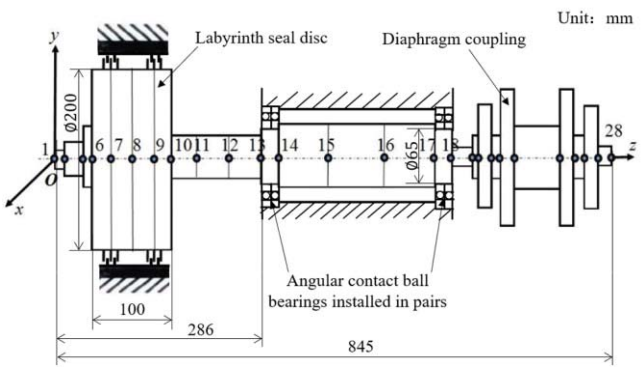

Figure 1. Model of labyrinth seal - rotor system

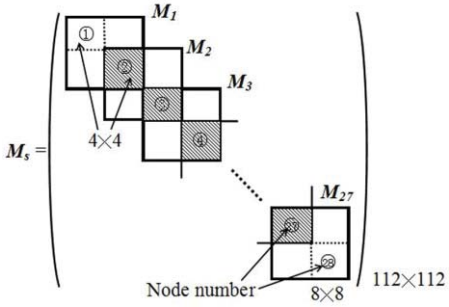

Figure 2. Assembly of matrix

The dynamic equation of the whole rotor system is:

$$\boldsymbol{M\ddot{u}} + (\boldsymbol{C} + \boldsymbol{D})\boldsymbol{\dot{u}} + \boldsymbol{Ku} = \boldsymbol{Q} \tag{2}$$

In the formula, $\boldsymbol{M}$ is the mass matrix of the rotor system, $\boldsymbol{D}$ is the gyro matrix and $\boldsymbol{K}$ is the stiffness matrix. The expressions of three matrix elements are given in reference [12]. In addition, $\boldsymbol{C}$ is the damping matrix of the system and $\boldsymbol{Q}$ is the combined external force vector.

$$\boldsymbol{C} = \boldsymbol{C_1} + \boldsymbol{C_2} \tag{3}$$

$$\boldsymbol{K} = \boldsymbol{K_1} + \boldsymbol{K_2} \tag{4}$$

$$\boldsymbol{Q} = \boldsymbol{F_p} + \boldsymbol{F_f} + \boldsymbol{G} \tag{5}$$

The damp matrix and stiffness matrix of the system in Equations (3-4) are composed of two parts, including the sum of the stiffness and damping matrices of the rotating shaft $\boldsymbol{K_1}$ and $\boldsymbol{C_1}$, and the bearing support stiffness and damping matrices $\boldsymbol{K_2}$ and $\boldsymbol{C_2}$. Since the adjacent two axes have common nodes, the $\boldsymbol{M}$, $\boldsymbol{K_1}$ and $\boldsymbol{D}$ matrices of rotor can be obtained by assembling the mass matrix as an example in the way of Fig. 2. The damping matrix $\boldsymbol{C_1}$ of the rotating shaft is proportional damping [9], which is a linear combination of $\boldsymbol{M}$ and $\boldsymbol{K_1}$. The expression is as follows:

$$\boldsymbol{C_1} = \alpha\boldsymbol{M} + \beta\boldsymbol{K_1} \tag{6}$$

In Equation (6), $\alpha = 4\pi f_1 f_2(\xi_2 f_1 - \xi_1 f_2) / (f_1^2 - f_2^2)$ and $\beta = (\xi_2 f_2 - \xi_1 f_1) / \pi (f_2^2 - f_1^2)$, ξ_1 and ξ_2 are the damping coefficient, which is the first and second order modal damping ratios; f_1 and f_2 are the first and second order natural frequencies (Hz).

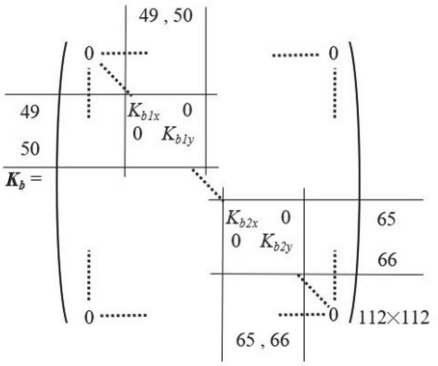

Figure 3. Supporting stiffness matrix structure

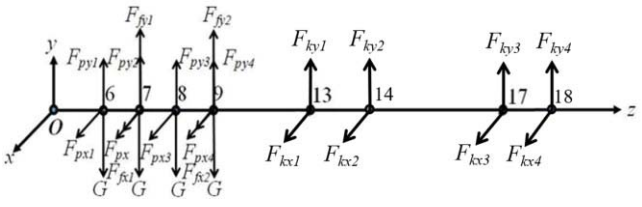

Figure 4. Drawing of rotor force

Supporting stiffness matrix $\boldsymbol{K_2}$ can be seen in Fig. 3. Supporting damping matrix $\boldsymbol{C_2}$ is the same as this form. In addition, in Equation (5), $\boldsymbol{F_p}$ is the eccentric force vector, $\boldsymbol{G}$ is the gravity vector, and $\boldsymbol{F_f}$ is the sealed force vector. The position of these nodes under the force of system is shown in Fig. 4.

B. Nonlinear Sealing Force Model

The Muszynska sealing force model [13-14] is adopted. The radial cross-sectional view of a sealing chamber is shown in Fig. 5. The circumferential angular velocity of the fluid near the rotor is ω, and near the stator is reduced to 0. The average circumferential velocity ratio of the fluid is expressed by τ, and the average velocity of the fluid in the sealing chamber can be expressed by $\tau\omega$. The disturbance reaction force of the seal force on the rotor rotates around it with the average flow velocity $\tau\omega$ along with the fluid. The rotation effect of the seal force is the main cause of the system instability. The specific expressions are as follows.

$$\begin{Bmatrix} F_{fx} \\ F_{fy} \end{Bmatrix} = -\begin{bmatrix} K - m_f\tau^2\omega^2 & \tau\omega D \\ -\tau\omega D & K - m_f\tau^2\omega^2 \end{bmatrix}\begin{Bmatrix} x \\ y \end{Bmatrix} - \begin{bmatrix} D & 2\tau\omega m_f \\ -2\tau\omega m_f & D \end{bmatrix}\begin{Bmatrix} \dot{x} \\ \dot{y} \end{Bmatrix} - \begin{bmatrix} m_f & 0 \\ 0 & m_f \end{bmatrix}\begin{Bmatrix} \ddot{x} \\ \ddot{y} \end{Bmatrix} \tag{7}$$

The expression of Muszynska seal force can be seen in Equation (4). K, D and m_f represent equivalent stiffness, equivalent damping and equivalent mass respectively. ω is the angular speed of rotor rotation. K, D and τ are all non-linear functions related to disturbance displacement x and y. They can be expressed as follows:

$$\begin{aligned} K &= K_0(1-e^2)^{-n} \\ D &= D_0(1-e^2)^{-n} \\ \tau &= \tau_0(1-e)^b \\ e &= \sqrt{x^2+y^2}/c \end{aligned} \qquad \begin{aligned} &n = 0.5\sim3 \\ &0 < b < 1 \\ &\tau_0 < 0.5 \end{aligned} \tag{8}$$

In Equation (5), parameters n, b and τ_0 are used to describe the specific sealing structure, the relative eccentricity of the rotor is expressed by e, the sealing clearance is indicated by c. K_0, D_0 and m_f in formula can be expressed as follows:

$$K_0 = \mu_0\mu_3, \quad D_0 = \mu_1\mu_3 T, \quad m_f = \mu_2\mu_3 T^2 \tag{9}$$

$$\mu_0 = \frac{2\sigma^2}{1+z+2\sigma} E(1-m_0),$$

$$\mu_1 = \frac{2\sigma^2}{1+z+2\sigma}\left[\frac{E}{\sigma} + \frac{B}{2}(E+\frac{1}{6})\right],$$

$$\mu_2 = \frac{\sigma\left(E+\frac{1}{6}\right)}{1+z+2\sigma}, \quad \mu_3 = \frac{\pi R\Delta P}{\lambda}, \tag{10}$$

$$T = \frac{l_m}{v_a}, \quad \sigma = \frac{\lambda l_m}{c}$$

Where the functions λ, E and B are respectively given in Equation (11):

$$\lambda = n_0 R_a^{m_0} \left[1 + \left(\frac{R_v}{R_a}\right)^2\right]^{\frac{1+m_0}{2}},$$
$$E = \frac{1+z}{1+z+2\sigma}, \tag{11}$$
$$B = 2 - \frac{\left(\frac{R_v}{R_a}\right)^2 - m_0}{\left(\frac{R_v}{R_a}\right)^2 + 1}$$

R_v and R_a denote the circumferential flow Reynolds number, and axial flow Reynolds number, respectively. There are:

$$R_v = \frac{R_m c \omega}{\gamma}, \quad R_a = \frac{2 v_a c}{\gamma} \tag{12}$$

In Equations (10-12), ΔP denotes the seal pressure difference, z denotes the entrance loss coefficient, γ denotes the hydrodynamic viscous coefficient, σ denotes the friction loss gradient coefficient, v_a denotes the axial flow velocity. R_m, c and l_m denotes the seal radius, clearance and length, respectively. The parameters are selected as follows: $\gamma = 1.3\times10^{-3}$ Pa·s, z=0.1, m_0=-0.025, n_0=0.079, τ_0=0.45, n=2, b=0.2.

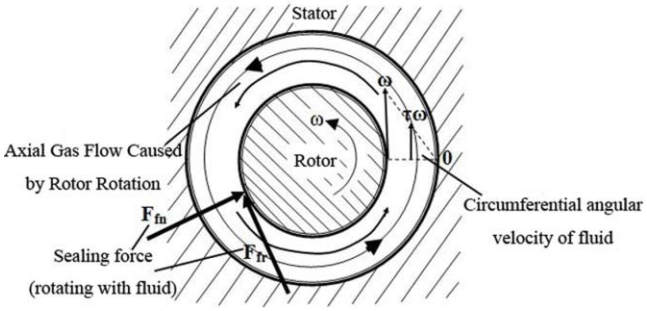

Figure 5. Schematic diagram of Muszynska sealing force model

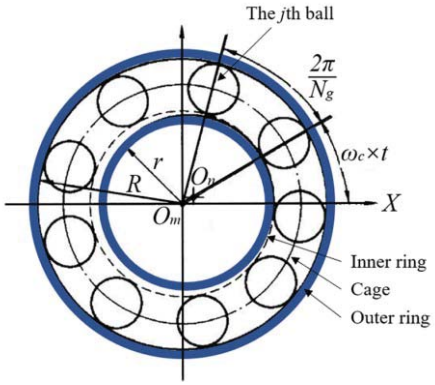

Figure 6. Schematic diagram of antifriction bearing

C. Rolling Bearing Force Model

The model of rolling bearing force in reference [15] is shown in Fig. 6. In this figure, N_b is the number of bearing balls, ω_c is the angular velocity of cage (i.e. ball center), R is the radius of bearing outer ring, r is the radius of inner ring, the supporting force of rolling bearing can be expressed as:

$$\begin{cases} F_x = \sum_{j=1}^{N_b} F_{jx} = \sum_{j=1}^{Nb} F_j \cos\theta_j \\ F_y = \sum_{j=1}^{N_b} F_{jy} = \sum_{j=1}^{Nb} F_j \sin\theta_j \end{cases} \tag{13}$$

F_j denotes the force on the j-th ball. Considering that only normal stress can be generated between the ball and the raceway, that is, the force can only be exerted when δ_j>0, step function H is introduced, and θ_j is the angular position of the j-th ball, which can be expressed by the following two formulas:

$$F_j = c_b \times \delta_j^a \times \mathrm{H}(\delta_j) \times \cos\alpha$$
$$\theta_j = \omega_c \times t + \frac{2\pi}{N_b}(j\text{-}1) \qquad j = 1,2,\cdots,N_b \tag{14}$$
$$\mathrm{H}(\delta_j) = \begin{cases} 1 & \delta_j > 0 \\ 0 & \delta_j < 0 \end{cases}$$

In Equation (14), α is the contact angle of the bearing, c_b is the Hertzian contact stiffness, its numerical value is related to the material and geometry of the ball and raceway; for ball bearings, a = 3/2, for roller bearings, a = 10/9; δ_j denotes the normal contact deformation between the j-th ball and raceway, which can be expressed by Equation (15). Due to the outer ring of the rolling bearing is fixed with the bearing seat, and the inner ring is matched with journal of rotor, the angular velocity at the cage can be expressed by Equation (16):

$$\delta_j = x\cos\theta_j + y\sin\theta_j - c_0 \tag{15}$$
$$\omega_c = \frac{\omega \times r}{R + r} \tag{16}$$

For the clearance of rolling bearing indicated by c_0 in Equation (15), the numerical value can be found in the mechanical design manual. The calculation parameters are shown in Table 1.

TABLE I. MAIN CALCULATION PARAMETERS OF ANTIFRICTION BEARING

Outer Ring Diameter *2R/mm*	Inner Ring Diameter *2r/mm*	Contact Stiffness Bearing C_b/(GN·m$^{-3/2}$)
100	65	10.5

III. Effect of Rolling Bearing Parameters on Rotor System Vibration

The Newmark-β method is used for numerical calculation to obtain the vibration response of the rotor. The main calculation parameters are as follows: the system material density ρ=7850Kg/m^3, the elastic modulus E=2.1×10^{11}Pa, the Poisson ratio v=0.3; the system damping coefficient ξ_1=0.02, ξ_2=0.04 [9]; The size of the selected seal structure are: c=0.1mm, l_m=15mm, ΔP=0.2Mpa, v_a=5m/s; the disc radius R_m=100mm, the disc length l=100mm, assuming eccentricity is occurred at the sealed disc only, which is 600g • mm.

The 7013C/DB angular contact ball bearings are used as the supporting parts of the system, N_b =14 and α =15°. The response in 7th point of the sealing teeth node at the left end of sealing disc is obtained when the rotational speed increases from 2000rev·min^{-1} to 10000 rev·min^{-1}. The bearing clearance value is determined by the tolerance zone between the inner ring of the rolling bearing and the rotating shaft. The clearance range of the rolling bearing is determined according to the bearing type in the mechanical design manual. Fig. 7 (a) and (b) are the bifurcation diagrams when without air flow excitation force and bearing clearance c_0 is taken as 3um and 20um respectively. Fig. 8 (a) and (b) are the bifurcation and waterfall diagrams of air flow exciting force when bearing clearance is 3um. Fig. 8 (c) and (d) are the bifurcation diagrams and waterfall diagrams of air flow exciting force when $c_0$is 20um. Fig. 9 (a) and (b) are the axle center trajectory and Poincaré section diagrams with/without air flow when c_0 is 20 um, respectively. It can be seen from Fig. 7 that the bearing clearance has a great influence on the dynamic behavior of the system.

When the bearing clearance increases from 3um to 20um, the stability of the system is poor. When the bearing clearance is small (c_0=3um), the system will lose stability due to the occurrence of air flow excitation after 5000 rev·min^{-1}, and make quasi-periodic/chaotic motion. From the three-dimensional waterfall diagram in Fig. 8 (b), it can be seen that the frequency f_f of air flow excitation remains unchanged at about 124.1Hz after 7300 rev·min^{-1}, that is, the phenomenon of frequency locking of air flow excitation occurs. At the same time, there are also have some combination frequency components, such as 1×-f_f, 2f_f, 1×+f_f, 1×+2f_f, 2×+f_f, 2×+2f_f, etc.

When the bearing clearance is large (c_0 =20um), the unstable vibration caused by the excessive bearing clearance can be suppressed to a certain extent by the air force at low rotating speed. The periodic-2(P-2)/P-n motion is started at 5400 rev·min^{-1} ~ 6600 rev·min^{-1}. The quasi-periodic/chaotic motion is carried out after 6600 rev·min^{-1}, and the vibration characteristics of the gas flow excited vibration are the main ones, as shown in Fig. 8 (c). From the 3D waterfall diagram of Fig. 8 (d), it can be seen that half-frequency components such as 1/2× and 3/2× are displayed at bearing clearance is 20um and speed is 5400 rev·min^{-1}~ 6500 rev·min^{-1},a short chaotic motion occurs between 6500 rev·min^{-1}and 7400 rev·min^{-1}. The frequency of the rotating speed after 7400 rev·min^{-1} is mainly composed of the air flow excitation frequency FF and its combination frequency.

Fig. 9 (a) and (b) show the axis trajectory diagram and Poincaré section diagram of the rotor system with/without air force at four node positions (node 7 is the left-end seal teeth at disc, node 9 is the right one; node 13 is the left-end bearing, and node 17 is the right bearing) when the speed is 10000 rev·min^{-1} and the bearing clearance is 20um. The Poincaré section is a closed curve composed of several points when there is no gas excitation force, which indicates that the system is in quasi-periodic motion at this time.

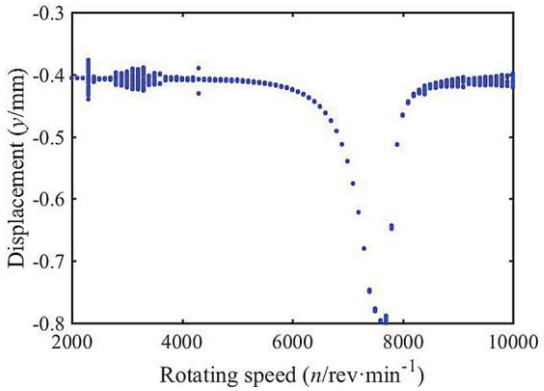

(a) Bearing clearance is 3um

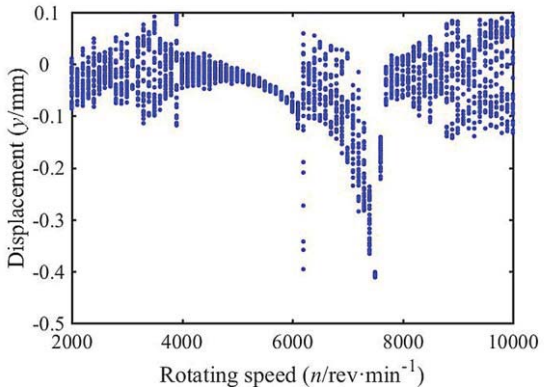

(b) Bearing clearance is 20um

Figure 7. Schematic diagram of antifriction bearing

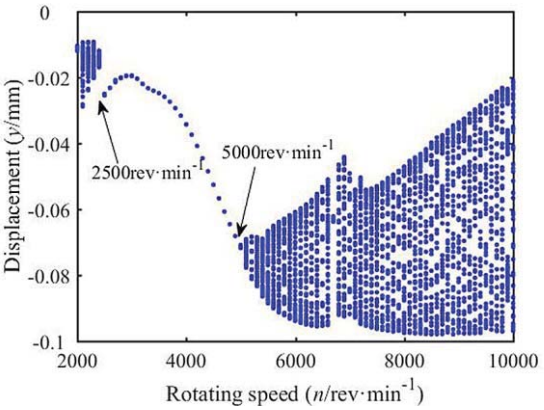

(a) Bifurcation diagram when bearing clearance is 3um

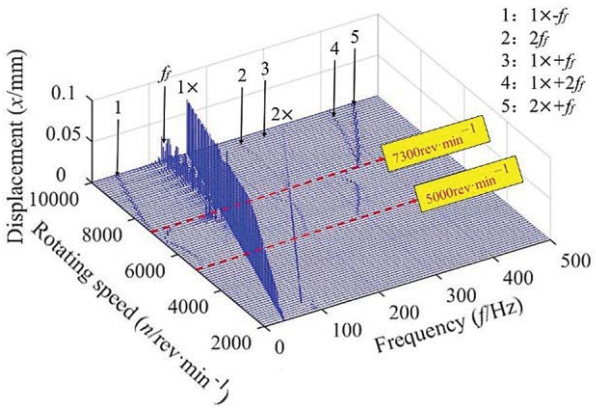

(b) The 3D waterfall diagram when bearing clearance is 3um

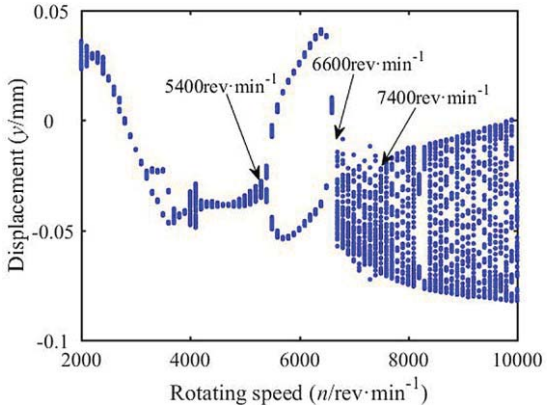

(c) Bifurcation diagram when bearing clearance is 20um

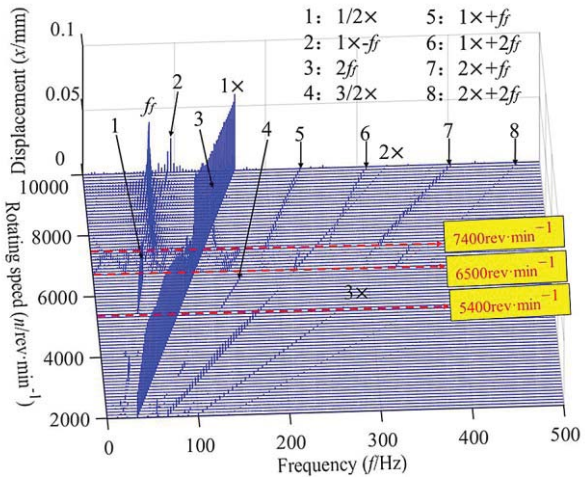

(d) The 3D waterfall diagram when bearing clearance is 20um

Figure 8. System response with sealing force

However, when considering the gas excitation force, the Poincaré section in each node is consist of scattered points, but at the sealed disc (nodes 7 and 9), the Poincaré section is a scatter point of approximately closed curve. In the bearing (node 13 and 17), the Poincaré section and the axis trajectory become more disordered. For the frequency spectrums from Fig. 9 (c) and (d), it can be found that frequency spectrum components at the bearing are more abundant than those at the disc, and there are half-frequency and combined frequencies related to air flow excitation frequency, such as $0.5\times$-f_f, $0.5\times$+f_f, $2f_f$ -$0.5\times$, $1.5\times$-f_f, etc. All of these indicate that the chaotic characteristics of the system are gradually strengthened due to the influence of air flow excitation on the bearing end.

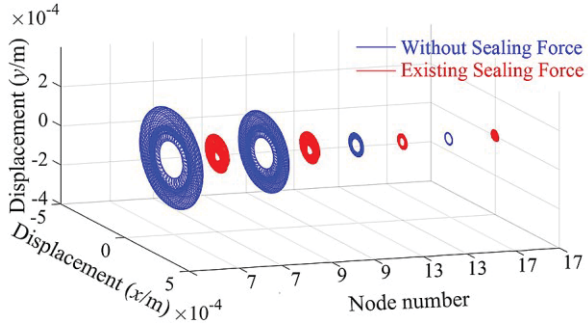

(a) Axis trajectory diagram at different nodes

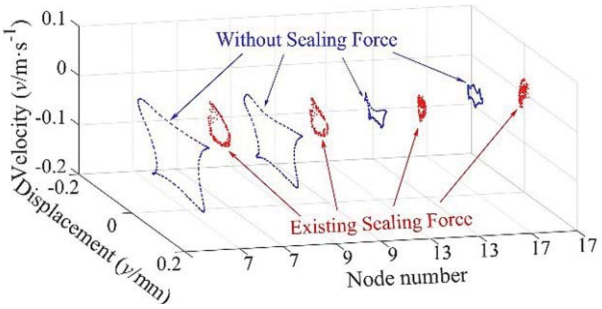

(b) Poincaré map at different nodes

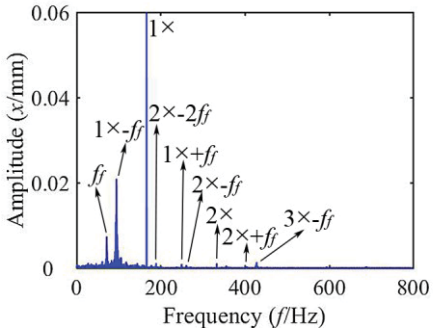

(c) Frequency spectrum at node 7

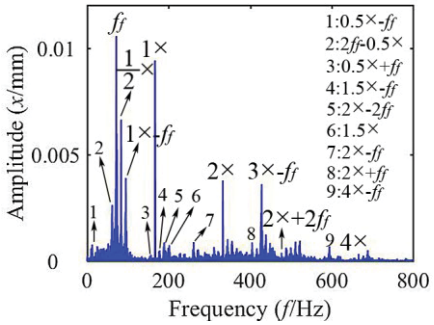

(d) Frequency spectrum at node 17

Figure 9. System response with sealing force

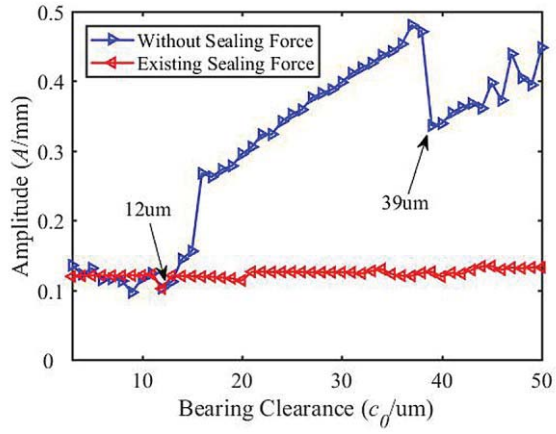

(a) Bearing clearance - amplitude curve

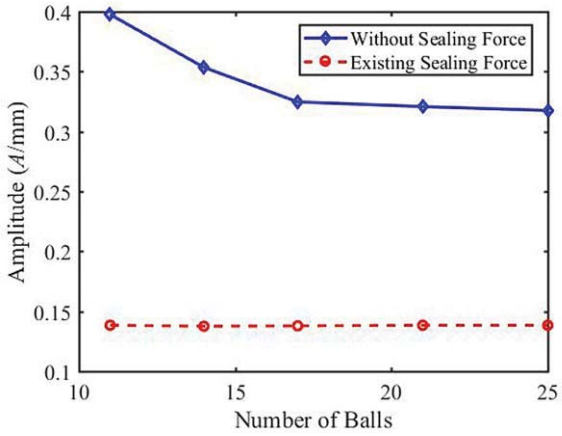

(b) Ball number-amplitude curve

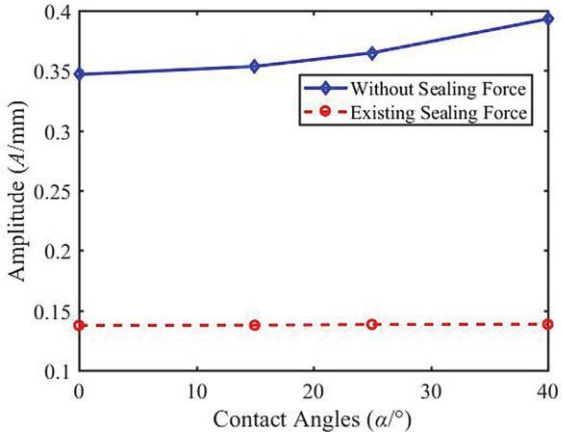

(c) Contact angle-amplitude curve

Figure 10. The influence of rolling bearing parameters on the system

When the rotational speed is stable at 10000 $rev \cdot min^{-1}$, and with or without airflow excitation force, Fig. 10 (a-c) shows the influence of bearing clearance, number of balls and contact angle on the disk amplitude (node 7). Fig. 10 (a) shows that the number of balls is 14 and the contact angle is 15°. The bearing clearance increases from 3um to 50um. It can be seen that the amplitude decreases slightly when without considering the airflow force, but increases sharply after 12um. Therefore, the appropriate tolerance zone can be selected in design and the processing accuracy of the shaft can be improved; In Fig. 10 (b), bearing clearance is 20um and contact angle is 15° are selected, balls number is 11, 14, 17, 21 and 25, respectively. When the number of balls increases from 11 to 17, the system amplitude decreases without considering the air force, but the amplitude decreases slightly when the balls number continues to increase after that. Therefore, from the perspective of vibration reduction, when the bearing model has been determined, the bearing with the appropriate balls number should be selected as the support component in the system; Fig. 10 (c) chooses bearing clearance is 20um and has 14 balls. Taking deep groove ball bearing 6013 (contact angle 0), angular contact ball bearing 7013C (contact angle 15), 7013AC (contact angle 25) and 7013B (contact angle 40) as examples, with the increase of contact angle, the radial amplitude will also raise, although the axial load that the bearing can bear will gradually increase. The bearing type with smaller contact angle should be selected to reduce the vibration while ensuring that the bearing can withstand the axial load. Considering the airflow excitation force, the vibration of rotor disc is mainly caused by the airflow excitation, and the bearing has a little influence.

ACKNOWLEDGMENT *(HEADING 5)*

The project supported by the Major Program of the National Natural Science Foundation of China (Grant No.51875085), and the Natural Science Foundation of Liaoning Province, China (Grant No. 20170540205, 20180551073).

REFERENCES

[1] Y. G. Luo, P. F. Wang, H. Xu, and C. Y. Wang, "Review and prospect on the research of the labyrinth seal – rotor system ," Journal of Dalian Minzu University, vol. 21, no. 1, pp. 6–14, January 2019.

[2] X. Yan, K. He, J. Li, and Z. P. Feng. "Numerical techniques for computing nonlinear dynamic characteristic of rotor-seal system," Journal of Mechanical Science and Technology, vol. 28, no.5, pp.1727–1740, May 2014.

[3] F. Cangioli, S. Chatterton, P. Pennacchi, L. Nettis, and L. Ciuchicchi. "Thermo-elasto bulk-flow model for labyrinth seals in steam turbines," Tribology international, vol. 119, pp.359–371, March 2018.

[4] S. Subramanian, A. S. Sekhar, and B. V. S. S. S. Prasad, "Rotordynamic characteristics of rotating labyrinth gas turbine seal with centrifugal growth," Tribology International, vol. 97, pp. 349–359, May 2016.

[5] D. Sun, S. Wang, Y. T. AI, K. M. Wang, Z. H. Xiao, Y. Li, and X. D. Yu. "Theoretical and experimental research on the performance of anti-swirl flow for the static and dynamic characteristics of seals," Journal of mechanical engineering, vol. 52, no.3, pp. 101–109, February 2016.

[6] X. W. Liu, G. Z. Zhang, C. Li, and M. Zhao. "Research on gas leakage pneumatic thermodynamic behavior in the radial labyrinth of scroll compressor," Journal of mechanical engineering, vol. 51, no.20, pp. 201–207, October 2015.

[7] W. Z. Wang, Y. Z. Liu, and P. N. Jiang, "Numerical investigation on influence of real gas properties on nonlinear behavior of labyrinth seal-rotor system," Applied Mathematics and Computation, vol. 263, pp. 12–24, July 2015.

[8] W. S. Ma, H. Huang, G. Q. Feng, Z. B. Chen, and R. G. Kirk. "Labyrinth seals diameter and length effect study on nonlinear dynamics", Procedia engineering, vol. 99, pp. 1358–1364, February 2015.

[9] H. Ma, H. Li, H. Q. Niu, R. Z. Song, and B. C. Wen, "Nonlinear dynamic analysis of a rotor-bearing-seal system under two loading conditions," Journal of Sound and Vibration, vol. 332, no.23, pp. 6128–6154, November 2013.

[10] E. J. Zhang, Y. H. Jiao, and Z. B. Chen, "Dynamic behavior analysis of a rotor system based on a nonlinear labyrinth-seal forces model," Journal of computational and nonlinear dynamics, vol. 13, no.10, pp. 101002–101002-12, July 2018.

[11] Y. G. Luo, B. Wu, H. W. Zhi, and Y. Q. Li, "Dynamics behaviours of labyrinth seal – sliding bearing – rotor system based on improved rub – impact force model," Journal of Dalian Minzu University, vol. 18, no.1, pp. 33–37, January 2016.

[12] H. Ma, et al., Dynamics of Rotating Blade-Casing Systems with Rubbing, Beijing: The Science Publishing Company, 2017.

[13] D. E. Bently and A. Muszynska, "Role of circumferential flow in the stability of fluid-handling machine rotors," Texas: NASA, pp. 1–5, May 1988 [The 5th Workshop on Rotor Dynamic Instability Problems in High Performance Turbo Machinery, May 16-18, 1988, Texas A & M University, Texas].

[14] Y. G. Luo, S. H. Zhang, B. Wu, and W. L. Wang, "Dynamic analysis on nonlinear fluid-structure interaction forces of rub-impact rotor system," Open Mechanical Engineering Journal, vol. 8, no.1, pp. 480-486, December 2014.

[15] Y. Q. Liu, B. S. Wang, and S. P. Yang, "Nonlinear Dynamic Behaviors Analysis of the Bearing Rotor System with Outer Ring Faults in the High-speed Train," Journal of Mechanical Engineering, vol. 54, no.8, pp. 17-25, April 2018.